ENGPHYS 4Z04 – Semiconductor Manufacturing Technology

Simulation Report

Instructor: Dr Gitanjali Kolhatkar

Muqtadir Hussain

400250481

Hussam43

Introduction:

The use of Technology Computer-Aided Design (TCAD) tools in the field of semiconductor device simulation has become essential for understanding and optimizing device performance. TCAD provides a robust platform for modeling, simulation, and analysis of electronic and photonic devices, including solar cells. Solar cells are semiconductor devices that convert light energy into electrical energy through the photovoltaic effect. They are a critical component in renewable energy technologies, enabling sustainable energy generation.

Sentaurus TCAD, developed by Synopsys, is a comprehensive suite of tools that facilitates the simulation of semiconductor processes and devices. It allows for detailed modeling of complex devices by incorporating physical models and material properties, offering significant advantages over other software platforms. Sentaurus stands out due to its capability to simulate multi-dimensional structures, handle advanced physical effects, and integrate various process and device simulation modules seamlessly. This enables researchers and engineers to gain insights into device behavior under different operating conditions and optimize designs for improved performance.

The motivation behind using TCAD, particularly Sentaurus, for solar cell simulation is to achieve an in-depth understanding of device characteristics such as current-voltage (I-V) behavior, optical response, and efficiency. Through these simulations, one can optimize design parameters, assess device performance before physical fabrication, and identify potential limitations or enhancements in device structure.

Materials and Methods:

The design and simulation of the solar cell were conducted using Sentaurus TCAD, a comprehensive suite of tools that facilitate the modeling and analysis of semiconductor devices. This simulation encompassed both fabrication and characterization processes, leveraging different modules within Sentaurus for a step-by-step approach to building and analyzing the solar cell.

The primary material used for this solar cell simulation was silicon, chosen for its widespread application in photovoltaic devices due to its optimal bandgap of approximately 1.12 eV, cost-effectiveness, and well-established processing techniques. The silicon substrate was doped with boron to create a p-type base with an initial concentration of 1×10^{14} atoms/cm^3. This doping level was chosen to establish a low-resistance substrate conducive to efficient carrier collection.

Sentaurus Process (SProcess) was used to simulate the fabrication steps involved in creating the device structure. The first step was the creation of the silicon substrate with defined dimensions: a width of 10 μm, height of 10 μm, and thickness of 50 μm. These dimensions were carefully selected to maintain computational feasibility while providing a realistic simulation domain. Adaptive meshing was employed, with an absolute error refinement factor of 2.5, to enhance the resolution in areas of interest, such as the junction and contact regions, ensuring accurate modeling of physical phenomena.

The wafer was initialized with a crystal orientation of ⟨100⟩, which is known for its favorable electronic properties, such as lower recombination rates and effective carrier transport. This orientation also aids in maintaining consistency with real-world manufacturing practices. Advanced calibration settings were applied, including dose control and backscattering activation, to ensure that ion implantation would closely mimic actual physical processes.

The ion implantation process was performed using phosphorus as the n-type dopant. Phosphorus was chosen due to its high diffusivity in silicon and its ability to create a well-defined n-type region. The implantation energy was set to 200 keV, and a dose of 1×10^{14} ions/cm^2 was used. A tilt angle of 7° was applied to minimize channeling effects, where dopant ions follow paths between atoms in the crystal lattice, potentially leading to non-uniform distribution. This step created a shallow junction essential for efficient light absorption and carrier collection.

The implanted dopants were then activated and driven into the silicon using a high-temperature diffusion process. The Charged Fermi model was chosen to simulate the diffusion of phosphorus, as it accounts for carrier concentration effects and provides accurate modeling of high-concentration regions. The diffusion temperature was set to 950°C, and the duration was 15 minutes. This step allowed the dopant to spread from its initial implantation site, forming a gradual p-n junction that optimized electric field distribution across the active region.

Following the diffusion process, an anti-reflection coating (ARC) was deposited. A 120 nm-thick layer of oxide was chosen for the ARC, applied using an anisotropic deposition process. This thin oxide layer was critical for reducing surface reflection and enhancing photon absorption into the silicon. The mechanical stress rebalancing feature was disabled to prevent stress-induced defects during this deposition process, which could negatively impact device performance. Additionally, the stress history was reset to ensure that no cumulative stress effects from earlier steps influenced the results.

Lithography was performed to define the areas where the top contact would be deposited. A mask was created with coordinates defining a rectangle on the wafer surface. This step was essential for selectively opening the oxide layer for metallization. A photoresist layer was applied with a thickness of 50 nm, and an anisotropic etch was used to remove the oxide layer within the masked region. This etching process provided the necessary window for the metal contacts while preserving the surrounding ARC.

The next step involved the deposition of the top contact materials. Titanium was deposited first as an adhesion layer with a thickness of 10 nm, followed by a 140 nm layer of silver, which served as the primary conductor due to its excellent electrical conductivity. Both materials were deposited anisotropically to maintain a uniform layer across the defined contact area. After metallization, the photoresist was stripped, leaving only the patterned metal contacts.

To create the rear contact, the wafer was flipped, and a 200 nm layer of aluminum was deposited anisotropically. Aluminum was selected for its low contact resistance and its ability to form a reliable ohmic contact with p-type silicon. Once the rear contact was deposited, the wafer was flipped back to its original orientation.

The device was then prepared for characterization using Sentaurus Device (SDevice). This module was configured to simulate the electrical and optical properties of the solar cell. The I-V characteristics were obtained by applying a voltage sweep at the anode, with the current collected from the cathode, allowing the extraction of key performance metrics such as open-circuit voltage and short-circuit current. The optical response was simulated using an illumination spectrum that replicated AM1.5G solar conditions, with data stored in am15g.txt.

To accurately model carrier transport and recombination within the solar cell, the simulation included the solution of Poisson's equation and continuity equations for both electrons and holes. The Fermi potential model was used, which accounts for the equilibrium distribution of carriers. Recombination processes were modeled using the Shockley-Read-Hall (SRH) method with doping dependence, as well as Auger and radiative recombination models to capture all potential loss mechanisms. Mobility was also defined with doping dependence to reflect the influence of carrier concentration on transport properties.

The mathematical solver was configured using the Incomplete Newton method for better convergence. This iterative solver handled up to 100 iterations with options for extrapolation, derivative control, and a relative error threshold to ensure numerical stability. The optical generation rate was computed using the Transfer Matrix Method (TMM) to accurately capture the effects of interference and absorption within the multilayer structure.

For visualization, various output files were generated, including .plt files for plotting I-V characteristics (IV_n2_des.plt) and spectral response (n2_spec_des.plt), as well as .tdr files (n2_des.tdr and n2_plot_des.tdr) for structural analysis and dopant profile visualization. These files were analyzed using Sentaurus Visual to confirm device behavior and assess carrier distributions, electric fields, and recombination rates.

Results and Discussion:

I-V Characteristics

The I-V curve obtained from the simulation (Figure 1) reveals the relationship between the current output and the applied voltage at the anode. This curve is essential for determining key performance metrics such as the open-circuit voltage and the short-circuit current. From the curve, the short-circuit current can be observed as the value of current when the voltage is zero, and the open-circuit voltage is identified at the point where the current drops to zero. These parameters are crucial for assessing the power output and efficiency of the solar cell.

The current response at the cathode, as depicted in the image (Figure 2) aligns with the expected characteristics of a solar cell. The negative current values reflect the flow direction, consistent with carrier collection at the cathode.

Spectral Response and Optical Generation

The spectral response of the solar cell, shown in Figure 3 "intensity vs wavelength" indicates the device's performance across various wavelengths. The response peaks between wavelengths corresponding to visible light, demonstrating that the anti-reflection coating (120 nm oxide) effectively minimizes reflection and enhances absorption in this range. The dips in the response may indicate areas where optical generation is less efficient due to absorption or material limitations.

Carrier Distribution and Doping Concentration

The donor concentration (Figure 4) and acceptor concentration (Figure 5) plots provide a comprehensive view of the doping profiles in the solar cell. The donor concentration plot shows a higher dopant density at the n-type region, while the acceptor concentration plot reflects the p-type base. These distributions are consistent with the intended p-n junction formation through ion implantation and diffusion processes.

The total doping concentration (Figure 6) combines the effects of both n-type and p-type dopants, showing a clear gradient from the surface to the bulk of the substrate. This gradient ensures the formation of an electric field at the junction, critical for charge separation and current generation.

Recombination Analysis

The total recombination rate plot (Figure 7) highlights the regions where recombination losses occur within the device. The color scale indicates higher recombination near the surface and junction areas, which could impact the overall efficiency. The analysis shows that while recombination is present, its distribution is relatively controlled, indicating that the device design effectively mitigates excessive carrier losses.

3D Schematic of the Simulated Device

The 3D schematics of the simulated device, as shown in the images for acceptor, donor, and doping concentration, illustrate the physical structure and dopant distribution. These plots provide visual confirmation of the successful formation of the p-n junction and validate the uniformity of the doping process across the device.

Data Assessment and Performance Evaluation

The results from the I-V curve, spectral response, and recombination analysis indicate that the solar cell exhibits typical behavior expected from a silicon-based photovoltaic device. The open-circuit voltage and short-circuit current derived from the I-V plot align with anticipated values for a silicon solar cell with similar doping concentrations and structural properties. The efficiency can be calculated by evaluating the maximum power point (MPP) from the I-V curve.

The spectral response confirms that the anti-reflection coating plays a significant role in improving light absorption, particularly within the visible spectrum. However, the recombination plot suggests potential areas for improvement, such as optimizing surface passivation to reduce surface recombination.

Efficiency:

- The I-V curve from Figure 1 shows a steep increase in current as voltage approaches its peak. Voc (open-circuit voltage) is approximately where the current becomes zero, and from the plot, this seems to be around **0.37 V**. Isc (short-circuit current) is where the voltage is zero, and the current appears to be around **0.045 A** from the plot. Vmpp can be estimated from the part of the curve where the product V×I seems to reach its highest point before the current drops sharply. Impp can similarly be estimated by observing where the current is at this maximum power point.

Based on the general shape of the I-V curve, Vmpp is typically around 70-80% of Voc. This suggests:

- **Estimated Vmpp:** 0.37 × 0.75 ≈ 0.28 V
- **Estimated Impp**: 0.045 × 0.75 ≈ 0.034 A

$$Pmax = Vmpp * Impp = 0.28\,V * 0.034\,A = \ 0.00952\,W$$

Pin is the input power, which, for standard test conditions (STC), is typically 1000 W/m^2 (1 sun) or 0.1 W.

$$n = \frac{0.00952}{0.1} = 9.52\%$$

<u>Conclusion:</u>

The simulation of the silicon-based solar cell using Sentaurus TCAD provided valuable insights into its electrical and optical performance. Through a comprehensive process that included ion implantation, diffusion, oxide deposition, and metallization, a realistic 3D structure of the solar cell was modeled and analyzed. The estimated maximum power point (MPP) indicated an efficiency of approximately 9.52%, which aligns with expected performance levels for standard silicon photovoltaic devices. The I-V curve analysis demonstrated typical behavior for a solar cell, with a well-defined Voc and Isc, suggesting that the doping profiles and junction formation were successful. The spectral response analysis highlighted effective photon absorption in the visible spectrum, bolstered by the anti-reflection coating, while the recombination rate distribution suggested manageable carrier losses, primarily occurring near the surface and junction regions. While the simulated solar cell performed adequately, areas for potential improvement include optimizing surface passivation techniques to reduce surface recombination and further refining the anti-reflection coating to enhance absorption across a broader range of wavelengths. Future work could explore the impact of different doping concentrations, alternative contact materials, or textured surfaces to improve the overall efficiency and performance.

<u>Appendix:</u>

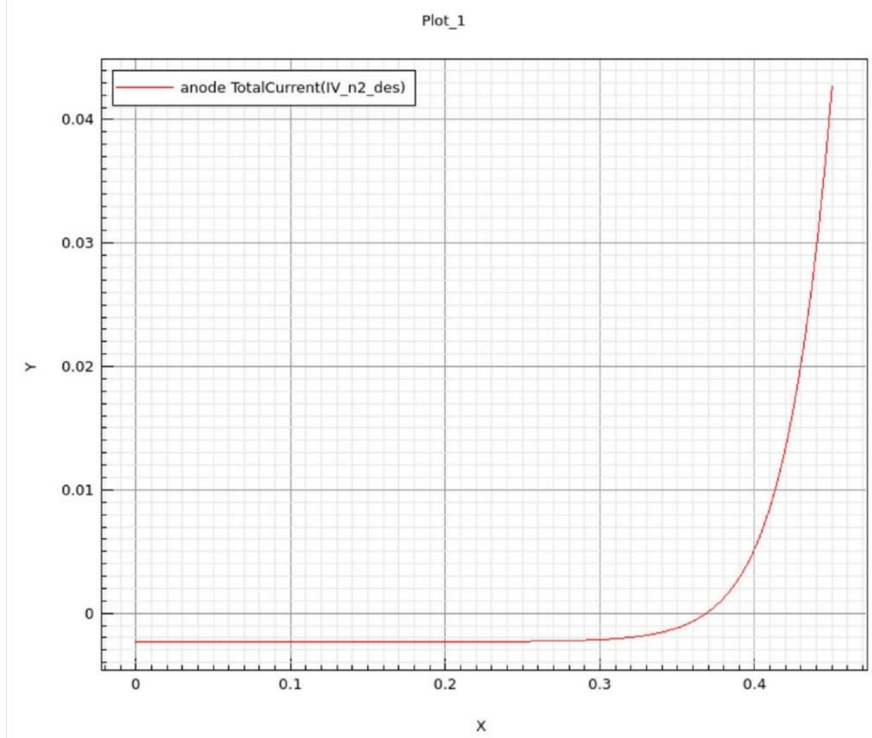

Figure 1

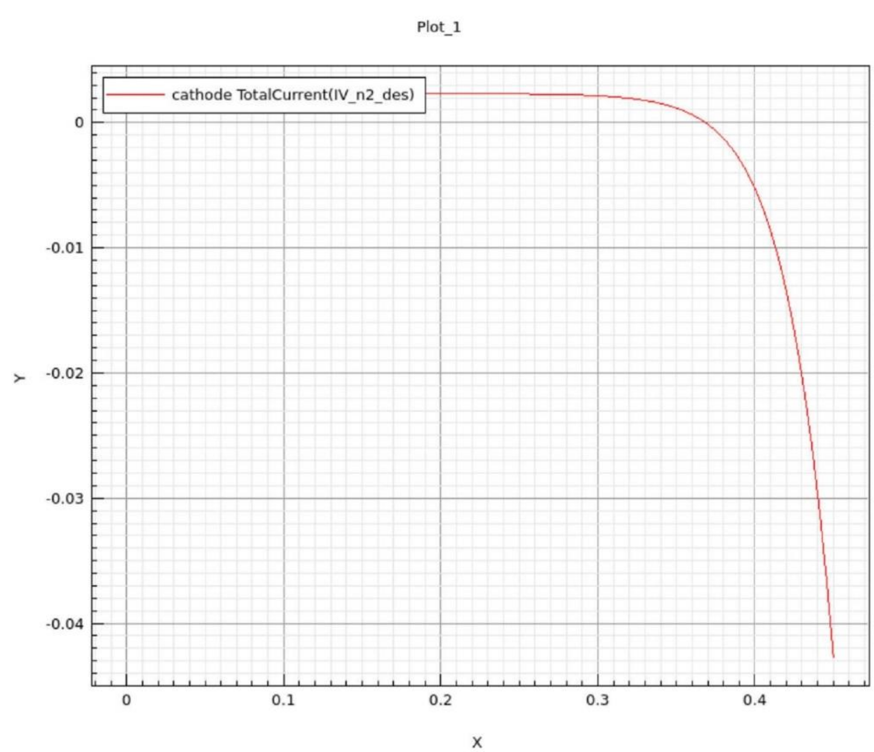

Figure 2

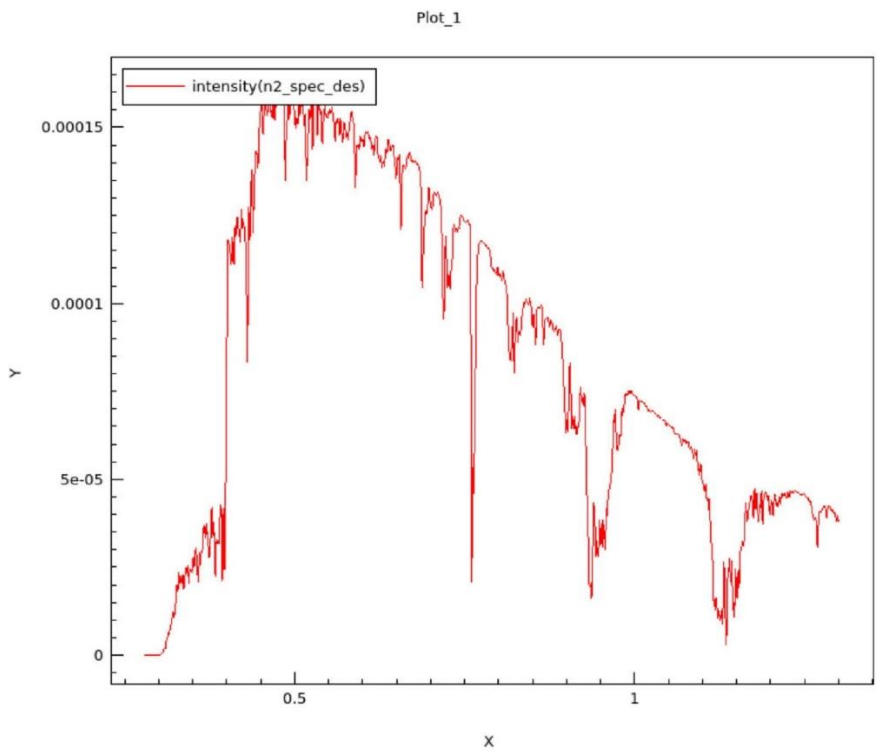

Figure 3

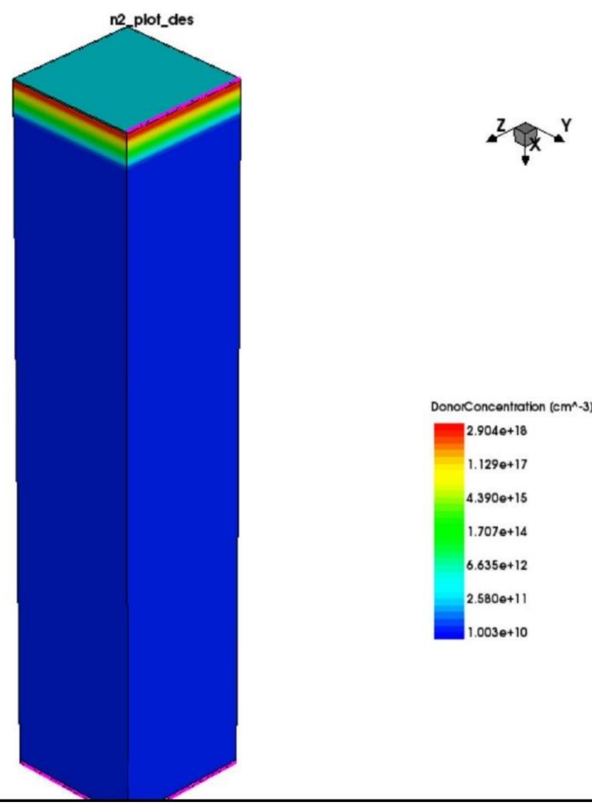

Figure 4

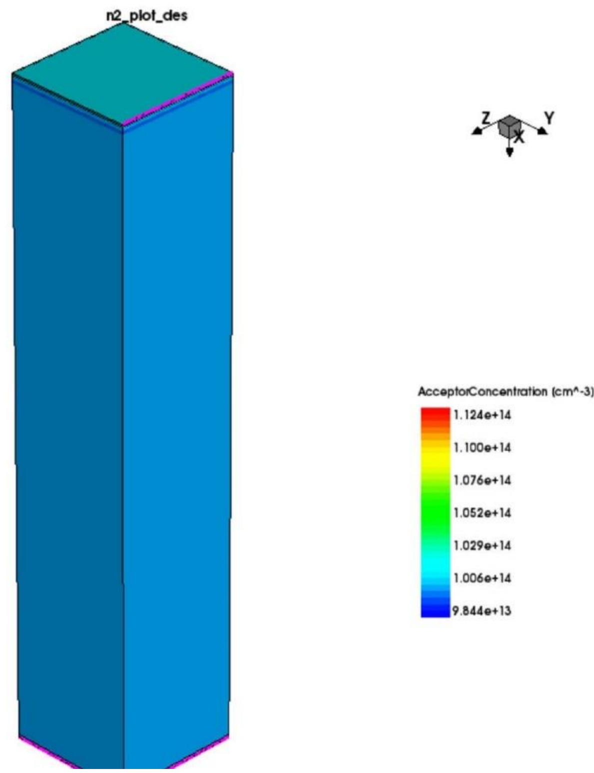

Figure 5

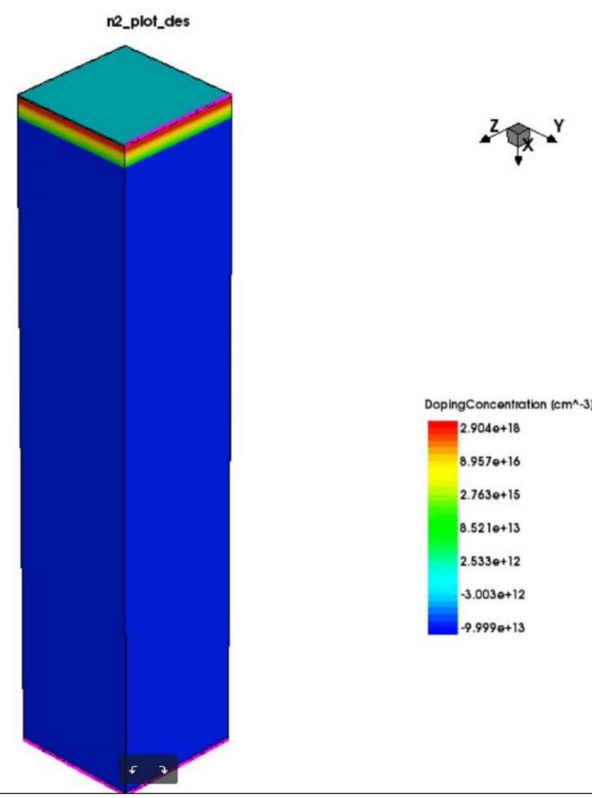

Figure 6

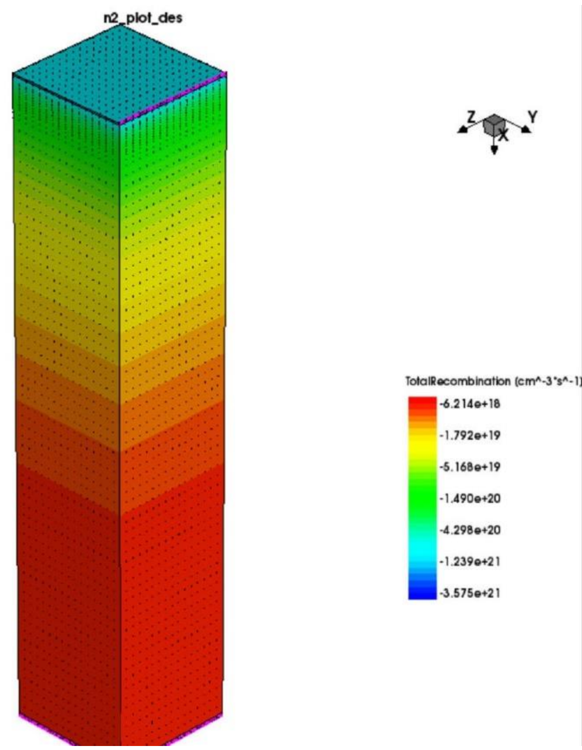

Figure 7

Code Part 1:

```
#### Step 1

## X lines
line x location= 0.0      tag= top
line x location= 50.0     tag= bot

## Y lines
line y location= 0        tag= left
line y location= 10.0     tag= right

## Z lines
line z location= 0        tag= front
line z location= 10.0     tag= back

## Create the silicon substrate
region silicon xlo= top xhi= bot ylo= left yhi= right zlo= front zhi= back

## Define the wafer orientation and base doping
init wafer.orient= 100 field= Boron concentration= 1e14

grid 3D
```

```
pdbSet Grid Adaptive 1
pdbSet Grid SnMesh UseLines 1
pdbSet Grid Silicon Refine.Abs.Error 2.5

AdvancedCalibration
pdbSet ImplantData DoseControl BeamDose

## Turn on Backscattering
pdbSet ImplantData TS4Backscattering 1


## Save the initial structure before implantation
struct tdr= n@node@_predose

#### Step 2

implant species=Phosphorus Silicon dualpearson tables= Tasch damage
implant Phosphorus energy=200 dose=1e14 Adaptive tilt= 7


SetPlxList Phosphorus
WritePlx n@node@_t0 y=5 z=5
pdbSet Grid Adaptive 1

struct tdr= n@node@_postdose_t0

#### Step 3
## diffusion
pdbSet Silicon Phosphorus DiffModel ChargedFermi
diffuse temperature= 950<C> time=15<min>


## make 1D dopant profile
SetPlxList Phosphorus
WritePlx n@node@_diffusion1 y=5 z=5

##Save structure
struct tdr= n@node@_diffusion1

#### Step 4
pdbSet Mechanics EtchDepoRelax 0
pdbSet Mechanics StressHistory 0

deposit Oxide thickness=0.12 type= anisotropic
```

```
struct tdr= n@node@_Step4

#### Step 5
## Create the Mask
point name= p1 coord= {9.99 0}
point name= p2 coord= {10 10}
polygon name= box1 points= {p1 p2} rectangle

mask name= m1 polygons= box1

## Refine the mesh to focus on areas around the mask
refinebox clear

# Prevent mesh propagation by defining regular coarse mesh
refinebox xrefine= 1 yrefine= 1 zrefine= 1

# Add edge-based refinement
refinebox mask= m1 mask.edge.mns= 0.08 mask.edge.refine.extent= 0.25
grid remesh

## Deposit photoresist
photo mask= m1 thickness= 0.05

## Etch the Oxide in the open window
etch Oxide type= anisotropic thickness= 0.12

struct tdr= n@node@_Step5

#### Step 6

deposit material=Titanium thickness= 0.01 type= anisotropic
deposit material=Silver thickness=0.14 type= anisotropic

## Remove photoresist
strip resist

struct tdr= n@node@_Step6

### Step 7
transform flip

deposit material=Aluminum thickness=0.2 type= anisotropic
```

```
transform flip

struct tdr= n@node@_Step7

## Step 8,9 & 10
# diffuse temperature= 450<C> time= 5<min> N2

contact name=anode bottom
contact name=cathode top

struct tdr= n@node@_scell
struct smesh= n@node@_scell_mesh
```

Code Part 2:

```
Electrode {
{ Name = "cathode" Voltage = 0.0}
{ Name = "anode" Voltage = 0.0}
}

File {
*- Input files:
Grid = "n1_scell_mesh_fps.tdr" IlluminationSpectrum =
"@pwd@/am15g.txt"
*- current/voltage results:
Current= "@plot@"
*- Spatial results:
Plot= "@tdrdat@"
*- Spectral results:
SpectralPlot = "n@node@_spec"
*- log files:
Output = "@log@"
OpticsOutput = "n@node@_optics"
}

Physics {
Area = 1e6
Fermi
Recombination( SRH(DopingDependence) Auger Radiative
surfaceSRH )
Mobility(DopingDependence)
Optics(
        ComplexRefractiveIndex ( WavelengthDep(Real Imag) )
        OpticalGeneration (
```

```
		QuantumYield(StepFunction(EffectiveBandgap) )
			ComputeFromSpectrum(
				Select(
		Parameter=("Wavelength")
					Condition="$Wavelength<= 1.3"
					)
				KeepSpectralData
				)
			)
		OpticalSolver (
			TMM (
				LayerStackExtraction ()
				Scattering()
				IntensityPattern = Envelope
				)
			)
Excitation (
		fromTop
		Window (Origin = (-3, 0, 0) Rectangle ( Corner1
= (0, 0) Corner2 = (3, 3) ))
			)
		)
}
Math {
IncompleteNewton
Iterations = 100
NotDamped = 100
Extrapolate
Derivatives
RelErrControl
Digits=10
}
Plot {
*- Optics:
OpticalIntensity
OpticalGeneration
*- Carrier Densities:
eDensity hDensity
EffectiveIntrinsicDensity IntrinsicDensity
eEquilibriumDensity hEquilibriumDensity
*- Currents and current components:
Current/Vector eCurrent/Vector hCurrent/Vector
eMobility hMobility eVelocity hVelocity
*- Fields, Potentials and Charge distributions
```

```
ElectricField/Vector Potential SpaceCharge
*- Generation/Recombination
srhRecombination AugerRecombination
RadiativeRecombination TotalRecombination
eLifeTime hLifeTime
RadiativeRecombination
*- Doping Profiles
Doping DonorConcentration AcceptorConcentration
*- Band structure
BandGap BandGapNarrowing ElectronAffinity
ConductionBandEnergy ValenceBandEnergy
eQuasiFermiEnergy hQuasiFermiEnergy
}
CurrentPlot{
OpticalGeneration(Integrate(Semiconductor) )
OpticalGeneration(Integrate(material="Silicon") )
srhRecombination(Integrate(Semiconductor))
AugerRecombination(Integrate(Semiconductor))
}
Solve {
*- Creating initial guess:
Coupled (Iterations = 100 LineSearchDamping = 1e-4){
Poisson }
Coupled (Iterations = 100){ Poisson Electron Hole }
NewCurrentPrefix= "tmp_"
Poisson
NewCurrentPrefix= "IV_"
*- Ramp to anode voltage to 0.45
Quasistationary (
	InitialStep =0.01 Increment = 1
	MinStep = 1e-3 MaxStep = 0.1
	Goal { Name = "anode" Voltage = 0.45 }
	)
{Coupled { Poisson Electron Hole }}
}
```